Interfacial instability as shaping mechanism for Polystyrene particles with tunable surface texture

Helena vom Stein, Dirk Volkmer

Angaben zur Veröffentlichung / Publication details:

Stein, Helena vom, and Dirk Volkmer. 2021. "Interfacial instability as shaping mechanism for Polystyrene particles with tunable surface texture." *Advanced Materials Interfaces* 8 (16): 2100628. https://doi.org/10.1002/admi.202100628.

ADVANCED MATERIALS INTERFACES
www.advmatinterfaces.de

Interfacial Instability as Shaping Mechanism for Polystyrene Particles with Tunable Surface Texture

*Helena vom Stein and Dirk Volkmer**

Surfactant-driven interfacial instability of emulsion droplets has recently emerged as a means for shaping polymeric particles with controllable surface texture. This paper presents a suspension polymerization-based method to produce surface-textured polystyrene particles by inducing an instability at the interface of prepolymerized emulsion droplets followed by rapid cooling. The interaction of two surface-active components, i.e., arachidic acid and cetyltrimethylammonium bromide (CTAB) at the phase boundary triggers the interfacial deformation at a specific point in time. Rapid cooling freezes the deformed emulsion droplets in a nonequilibrium state. Viscosity is proposed as the key parameter influencing the particle morphology, which can be controlled by easily adjustable factors such as initiator concentration, temperature, time, and cooling rate. Contact angle hysteresis measurements of particle thin layers spread on a flat substrate reveal a strong influence of the particle surface texture on the wetting behavior. The presented particle synthesis method requires no specialized equipment and has a high potential for upscaling, making it promising for various applications including hydrophobic coatings, catalyst supports, separation technology, tissue engineering, or drug delivery.

1. Introduction

In recent years, both fundamental and applied research have devoted a great deal of effort to the design and precise control over microparticle size, shape, and surface texture.[1] This interest stems from the fact, that the morphology significantly affects the particles' physical properties and plays a substantial role in many applications, including drug delivery,[2] tissue engineering,[3] catalysis,[4] and separation.[5] The ever-increasing demand for application-specific particle performance and the requirements that have to be met for an economic upscaling cause a continuous search for new synthesis methods.

Quite recently, considerable attention has been focused on the use of dynamic self-organization processes at the phase boundary of immiscible liquids as a means to structure particles. In the underlying mechanism, often termed "spontaneous emulsification," the adsorption of surface-active ingredients at the interface of immersed droplets gives rise to vanishing or transiently negative surface tensions.[6] This causes an expansion of the surface area leading to buckling, droplet break-off, and ultimately the formation of a microemulsion. Through careful choice of chemical components and process parameters, the deformation can be trapped in a nonequilibrium state at which the surface is corrugated. Nanoparticles and microparticles of various sizes and shapes can be obtained, depending on whether the attention is drawn to the ejected submicroscopic droplets or the macroscopic mother droplet.[7]

The overall strategy for shaping particle surfaces through an interfacial instability is to slow down reaction kinetics such that a nonequilibrium state is frozen. Recent works have reported on a temperature-dependent shaping of oil droplets, which is based on the formation of a crystalline surfactant monolayer at the surface of emulsion droplets. Through an interfacial instability that occurs upon cooling, the liquid droplets pass through a series of complex regular shapes.[8] Those faceted droplets can then be polymerized by UV-irradiation to obtain solid particles.[9]

Another study reports on dendritic inorganic particles, which are obtained through an interfacial instability by including small quantities of a monomeric metal oxide precursor into oil droplets suspended in water.[10] The precursor condenses at the oil/water phase boundary upon contact with water and forms fragile and complex-shaped mineralized hollow shells. Other recent investigations have succeeded in preparing rough polymeric particles by an approach that employs solvent evaporation from microfluidic droplets containing an amphiphilic diblock copolymer to induce an interfacial instability.[11] In this approach the bulk viscosity of the droplets increases upon solvent evaporation, which eventually stops the deformation. The procedure typically requires evaporation of solvent from droplets lying on the ground of a vessel through an overlying continuous aqueous phase. This step requires very low liquid levels or long time spans both of which are unfavorable for or even impede upscaling purposes. To overcome these constraints,

H. vom Stein, Prof. D. Volkmer
Solid State and Materials Chemistry
University of Augsburg
Universitaetsstrasse 1, D-86159 Augsburg, Germany
E-mail: dirk.volkmer@physik.uni-augsburg.de

The ORCID identification number(s) for the author(s) of this article can be found under https://doi.org/10.1002/admi.202100628.

DOI: 10.1002/admi.202100628

we developed a nonevaporation induced procedure to prepare rough polymeric particles by simple suspension polymerization and quenching. Triggering the interfacial instability is achieved by a combination of amphiphilic arachidic acid and cetyltrimethylammonium bromide (CTAB).

In this paper, we present interfacial deformation of pre-polymerized monomer droplets for the preparation of microscopic polymer particles. We report on the influence of process parameters such as temperature, radical initiator concentration, time, and cooling rate on the resulting surface texture and identify viscosity as the key parameter. Our strategy requires no specialized equipment and has a high potential for upscaling, making it promising for various applications, including hydrophobic coatings, catalyst support, separation technology, tissue engineering, and drug delivery.

2. Results and Discussion

2.1. Formation of Rough Particles by Freezing of Deformed Emulsion Droplets

The interface of a nonpolar emulsion droplet containing arachidic acid and an aqueous phase containing cationic CTAB exhibits an interfacial instability, which features spine formation, droplet break-off, and ultimately the formation of a microemulsion.[10a] Right before the onset of the interfacial deformation, arachidic acid molecules cover the surface of the oil droplets. In contact with water, the arachidic acid molecules dissociate and become negatively charged.[12] Amphiphilic CTA^+ cations penetrate into the arachidic acid loaded interface, which causes a drastic decrease in interfacial tension. At a certain point, the interfacial tension reaches extremely small or even transiently negative values.[6] This causes the interface to become unstable and the interfacial area to increase by growing spines and ejecting tiny droplets.

We produce rough polystyrene particles by inducing the described surfactant-driven instability at the interface of pre-polymerized emulsion droplets. The particle formation mechanism is illustrated in **Figure 1**. The preparation procedure can be subdivided into three major steps

1. Pretreatment of monomer droplets through suspension polymerization
2. Initiation of the interfacial instability
3. Preservation of the particle structure by rapid cooling of the dispersion

In the first step, the nonpolar phase consisting of styrene monomer, free-radical initiator azobisisobutyronitrile (AIBN), and arachidic acid is pretreated by free-radical polymerization. This is achieved by employing suspension polymerization, in which polymerization takes place within droplets in a continuous phase of ultrapure water. After a predefined polymerization time, where the droplets are still in a liquid state, the emulsion is added to a cold aqueous solution of CTAB. The sudden presence of the CTAB molecules triggers the interfacial instability at the surface of the polymer droplets. Simultaneously fast cooling of the emulsion increases the polymer viscosity, which significantly reduces the deformation rate. The polymerization continues at low temperature allowing the system

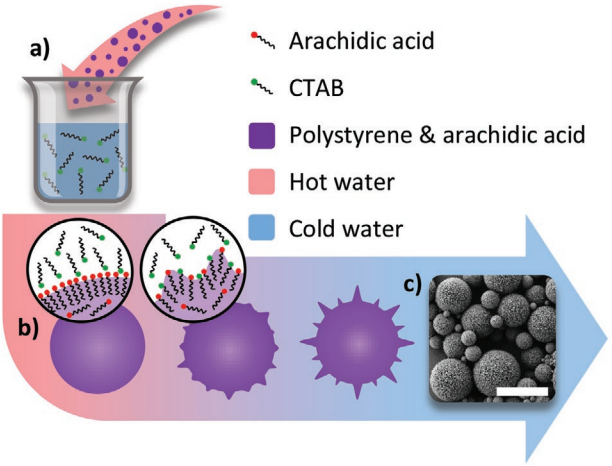

Figure 1. a) Addition of a 70 °C hot emulsion of pre-polymerized styrene droplets containing arachidic acid to a cold cetyltrimethylammonium bromide (CTAB) solution triggers the spontaneous emulsification. b) Spine formation during spontaneous emulsification. Insets show cationic CTAB molecules penetrating into the arachidic acid-loaded interface inducing the bending of the interface. Simultaneous cooling of the emulsion freezes the deformed polystyrene droplets in their nonequilibrium shape. c) The scanning electron image shows polydispersed surface-textured polystyrene particles with a scale bar of 50 µm.

to become kinetically trapped in the complex, nonequilibrium structure. In the following, we identify the major parameters having a direct impact on the morphology and surface texture of the resulting particles.

2.2. Factors Influencing the Particle Morphology

2.2.1. Polymerization Temperature and Initiator Concentration

The required polymerization time leading to structured particles is very sensitive to polymerization temperature and concentration of free-radical initiator AIBN. The influence of these parameters was tested according to the conditions listed in **Table 1**. For this purpose, test samples were withdrawn from the ongoing suspension polymerization and added to the aqueous CTAB solution after certain time intervals. The duration of polymerization periods leading to structured particles is given in terms of starting point and time span and is evaluated by optical microscopy. Increasing polymerization temperatures

Table 1. Required polymerization times leading to structured particles with variation of polymerization temperature and concentration of initiator c_{AIBN}.

Condition	Temperature [°C]	c_{AIBN}[a)] [wt%]	Onset[b)] [min]	Time span [min]
I	60	1	174 ± 7	61 ± 15
II	70	1	113 ± 4	30 ± 5
III	80	1	90 ± 5	9 ± 4
IV	80	2	75 ± 2	6 ± 3
V	80	3	67 ± 4	5 ± 2

[a)] c_{AIBN} is given in weight percent with respect to the monomeric phase;[b)] Minimum polymerization time to achieve structured particles.

(conditions (I) to (III)) as well as increasing radical initiator concentrations (conditions (III) to (V)) lead to an earlier onset and a shorter time span in terms of achieving structured particles.

2.2.2. Polymerization Time

Within the time span leading to structured particles the resulting morphology is continuously changing and evolves with time. Various kinds of microstructures on the particle surfaces were obtained by variation of polymerization times between 112 and 144 min (condition (II) in Table 1). **Figure 2** depicts light microscopy images and scanning electron images of particles with different morphologies. Particle morphologies were classified into five different morphological categories, hereafter denoted as category A, B, C, D, and E. Due to light scattering, polystyrene particles with a very rough surface appear black under the light microscope, particles with a smoother surface structure appear translucent. Suspension polymerization generally produces broad particle size distributions with an average size between 10 and 100 µm.[13] However, we found that the surface morphology is, to a large extent, independent of droplet size. Figure 2 illustrates, that the evolving surface texture becomes finer upon increasing the pretreatment time. The estimated value of the distance of the developed protrusions lies between 2 and 3 µm for category A and gradually decreases with increasing polymerization time to about 0.3 µm for category E.

We investigated the bulk structure of the particles by means of focused ion beam (FIB) milling. **Figure 3** shows false color scanning electron images of the particle cross sections. It illustrates that, for particles of category D, the microstructure is restricted to the particle surface and the particle's core is a solid sphere. However, for particles of category B the convolutions that make up the microstructure reach deep down into the particle center.

2.2.3. Monomer Conversion Determines Viscosity Increase upon Cooling

The influence of the presented parameters temperature, initiator concentration, and polymerization time suggests, that there is a strong correlation between the obtained particle morphology and the monomer conversion in the polymer solution. Over the course of the polymerization, the number of polymer chains as well as their length increases. Furthermore, polymerization accelerates with increasing temperature

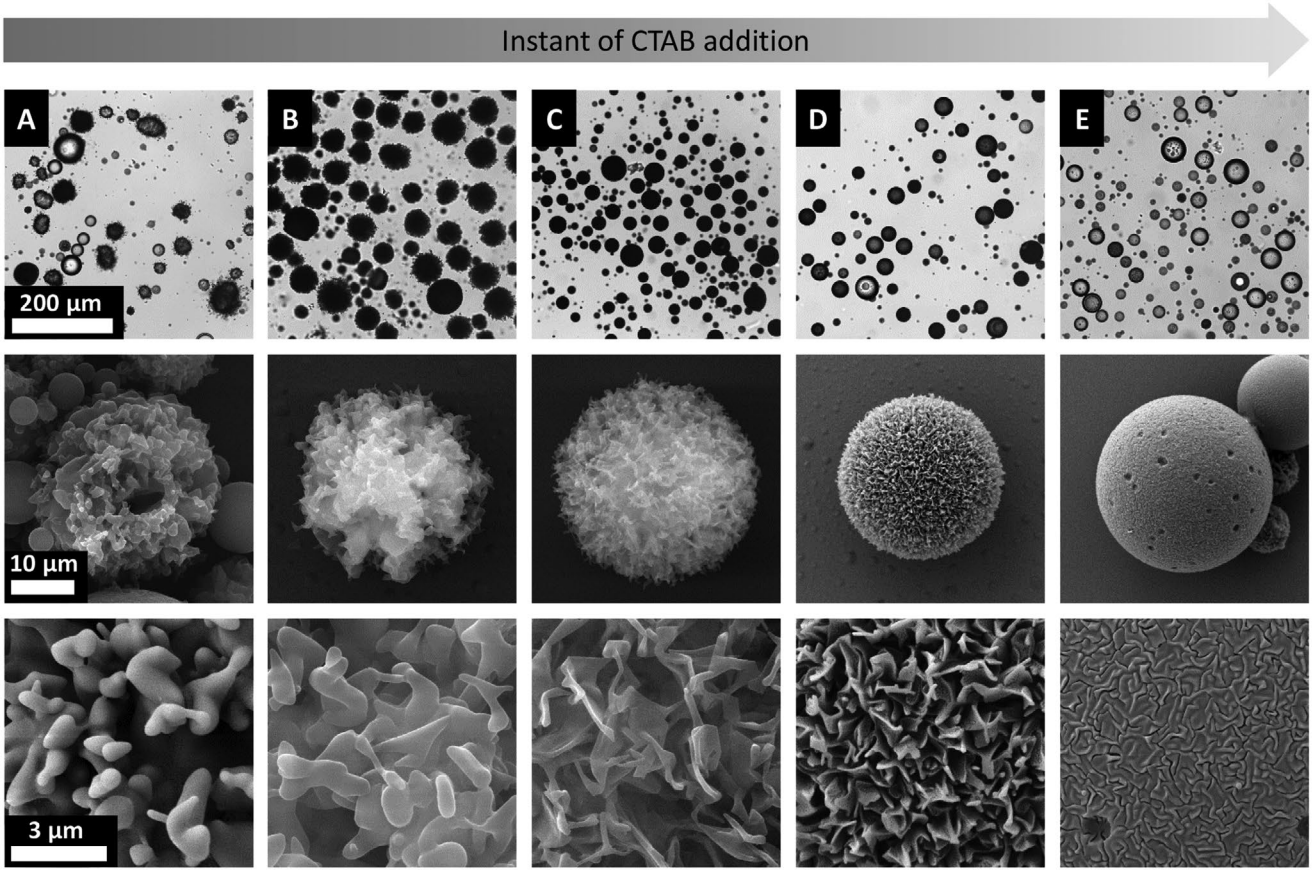

Figure 2. Polystyrene particles prepared by suspension polymerization at 70 °C and an initiator concentration of 1 wt% (condition II). The microstructure on the surface depends on the prepolymerization time at the instant of CTAB addition. From left to right with increasing total polymerization times before CTAB addition: A) 112 min, B) 120 min, C) 128 min, D) 136 min, and E) 144 min. Top row: photomicrographs. Middle row: scanning electron images of single particles. Bottom row: close-up view of particle surface. The scale bars are valid for the entire row.

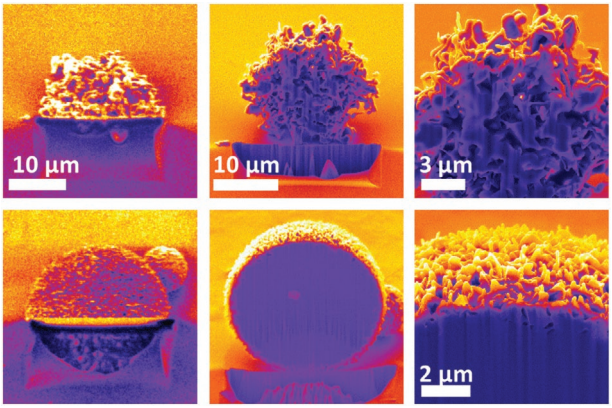

Figure 3. False color scanning electron images of FIB-milled cross sections of representative particles prepared by suspension polymerization at 70 °C and an initiator concentration of 1 wt% (condition II). First row: polymerization time 120 min (category B). Second row: polymerization time 136 min (category D). From left to right: FIB-image top view, secondary-electron image of particle cross section from an angle of 54°, close-up view. Scale bars are valid for upper and lower row unless otherwise stated.

and initiator concentration.[14] It is a well-known fact, that an increasing polymerization degree as well as an increasing number of polystyrene molecules in a solvent, styrene in our case, increases the viscosity of a polymeric solution.[15] Furthermore, temperature has a strong impact on the viscosity of a concentrated polymer solution, which becomes more pronounced with increasing polymer concentration.[16] We propose that the variations in the viscosity of the polymeric phase are responsible for the development of the different particle morphologies and surface textures. **Figure 4** displays the temperature dependence of the shear viscosity of polymer solutions that were pretreated at 70 °C for different amounts of time

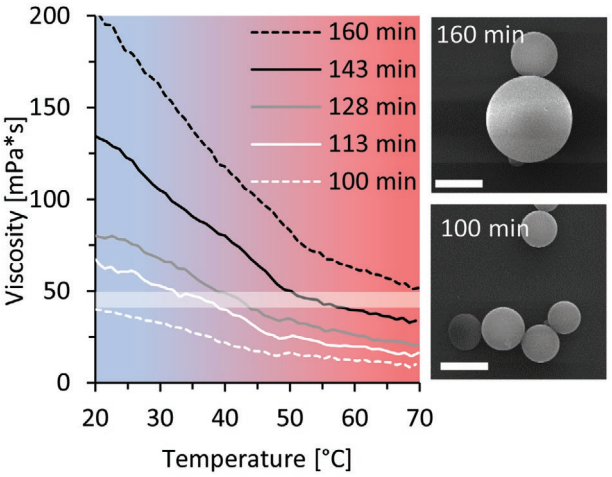

Figure 4. Temperature dependence of the shear viscosity of polymer solutions prepared by bulk polymerization at 70 °C for different time spans (condition II). Solid lines represent conditions where, uniformly rough particles are obtained (see Figure 2 category A, C, and E). Dashed lines represent preparations resulting relatively smooth particles. Scale bars are 10 µm.

(condition (II) in Table 1). The viscosity of all polymer solutions strongly increases with decreasing temperature.

The emergence of different surface textures with variation of the polymerization time can be explained by virtue of an increasing polymerization degree and the associated viscosity behavior upon cooling. The viscosity increase of the polymer phase during cooling determines how far the deformation can proceed before the polymerization of the particles is completed, because higher viscosities significantly reduce the interfacial deformation rate. The most homogeneous rough particles are obtained if the viscosity upon cooling passes through values of 40–50 mPa s. At polymerization times of 100 min and below, the viscosity upon cooling remains below that value and the emulsion droplets undergo spontaneous emulsification before the droplets are fully polymerized. In this case, submicroscopic droplets detach from the interface and the interface returns to its equilibrium shape, which is a smooth spherical surface. In contrast, viscosities surpassing values of 40–50 mPa s even before cooling significantly reduce the interfacial deformation rate, so that little or no surface structuring is observed in the final particles (160 min). For a polymerization time of 143 min (category E in Figure 2), a viscosity of 40–50 mPa s is reached at temperatures of 50–60 °C and therefore quickly after the surface deformation is initiated. In this case, the particles exhibit finer surface structures that represent the beginning formation of surface asperities. The opposite is true for a polymerization time of 113 min (category A in Figure 2), where the viscosity reaches 40–50 mPa s at temperatures between 30 and 40 °C and coarser structures result, thus representing a later stage of spontaneous emulsification.

We have shown that increasing polymerization temperatures as well as increasing radical initiator concentrations lead to an earlier onset and a shorter time span in terms of achieving structured particles. With increasing polymerization temperatures and radical initiator concentrations the polymerization accelerates and shorter polymerization times are required to obtain a polymer solution whose viscosity increases to above 40–50 mPa s upon cooling.

2.2.4. Cooling Rate

The strong influence of the temperature on the polymer solution viscosity suggests that the cooling rate is another important factor that has an impact on the particle morphology. Although the interfacial instability and cooling of the suspension are initiated at the same time, cooling is not instantaneous and the deformation proceeds to a certain degree before the shape of the droplets freezes due to the high viscosity. The influence of different cooling rates on particle morphology is shown in **Figure 5**. It should be noted, that the temperature was measured in the continuous phase and does not necessarily represent the temperature inside the droplets, which is rather higher. Different cooling rates were achieved by adding the hot emulsion directly to a CTAB solution stored in water baths of 20, 15 °C, or in an ice bath. With higher cooling rates, more particles are textured and the spiny morphology becomes denser. Lower cooling rates produce less structured particles or cloudy suspensions with detached submicroscopic droplets.

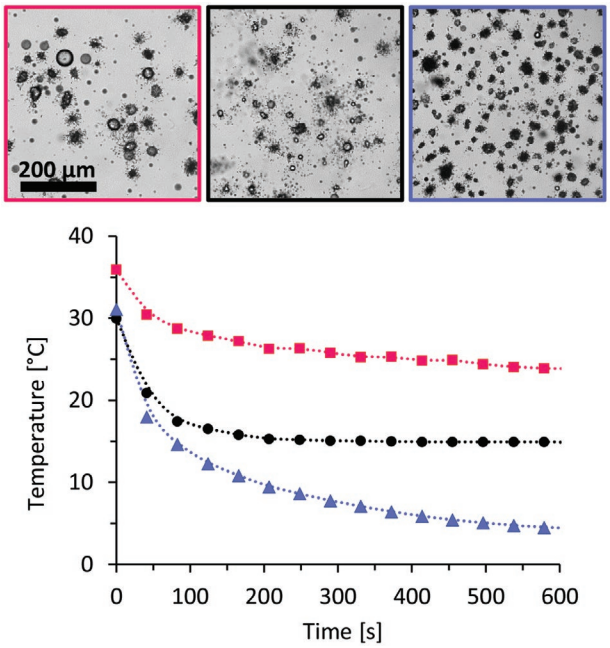

Figure 5. Influence of the cooling rate on the particle morphology. The light images show particles obtained from CTAB addition after 124 min of polymerization at 70 °C and different quenching conditions. Fast cooling produces densely structured particles (blue). Lower cooling rates produce less structured particles (red) or cloudy suspensions with detached submicroscopic droplets (black).

This is in qualitative agreement with the morphological evolution with decreasing polymerization time. Through a high cooling rate, the viscosity of the droplets increases more rapidly and the process of spontaneous emulsification stops at an earlier stage. Through a low cooling rate, the viscosity of the droplets increases slowly, trapping the particles in a later stage of spontaneous emulsification. This includes cloudy suspensions, in which submicroscopic droplets have already detached from the mother droplets. Fluid volume and vessel geometries have a major impact on the heat flux, which is why the control of the cooling rate is essential for the scalability of the process.

2.3. Wetting Behavior Changes with Morphology

Contact angle measurements reveal, that the dynamic wetting behavior of films of particles with the different morphologies depicted in Figure 2 changes drastically. With rough samples, it is convenient to measure contact angle hysteresis instead of static contact angle. Contact angle hysteresis indicates the difference between the advancing and receding contact angle that evolves when the volume of a droplet of a test medium sitting on the sample's surface is increased and decreased. Contact angle hysteresis on rough samples arises from pinning of the droplet contact line at surface asperities. Large values of hysteresis arise if a droplet is placed on a rough surface and the asperities are completely engulfed in the liquid, the so-called Wenzel state. On the other hand, in the Cassie–Baxter state, a droplet sitting on top of the asperities trapping air pockets between the droplet and the solid surface exhibits large contact angles but

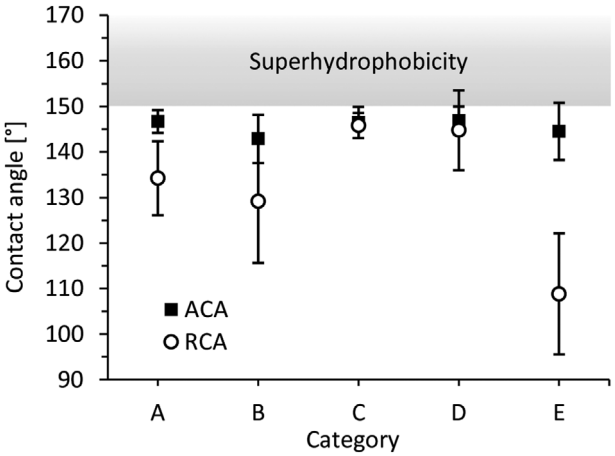

Figure 6. Advancing contact angles (ACA) and receding contact angles (RCA) of particle films prepared from particles with different surface textures corresponding to morphologies shown in Figure 2. The gray area indicates the region of superhydrophobicity, which starts at 150°.

small hysteresis. Low contact angle hysteresis paired with low surface energy features highly mobile droplets and is typical for superhydrophobic materials with self-cleaning properties such as the lotus leaf.[17] **Figure 6** shows the contact angle hysteresis of the different particle morphologies described above in terms of advancing and receding contact angle. The advancing contact angle changes little over the different surface textures and ranges from 143° to 147°. However, significant changes of the receding contact angle result in very small contact angle hysteresis of morphologies of category C and D. Droplets on these samples are extremely mobile and roll off easily when the surface is tilted. This behavior qualitatively resembles superhydrophobic materials with self-cleaning properties and is assigned to a Cassie–Baxter state in which a droplet contacts only the tip of the asperities trapping air pockets underneath. All other categories (A, B, and E) show significant contact angle hysteresis. Here, the particle–water contact area is larger than for the previous case, which results in a higher droplet adhesion.

3. Conclusion

We have demonstrated a suspension polymerization-based method that uses surfactant-induced interfacial instability and rapid cooling to produce rough polymer particles that represent the nonequilibrium shape of deformed emulsion droplets. We have identified viscosity as the key parameter influencing the particle morphology, which can be tuned by initiator concentration, temperature, polymerization time, and cooling rate. The method can most likely be employed to numerous other materials such as other monomers or inorganic precursors, because besides the described surfactants simply a sudden increase of viscosity or a solidification reaction is needed to preserve the morphology. The method has a high potential for upscaling, because it employs suspension polymerization, which is used on an industrial scale for bead production of various polymers.[13] Scaling requires precise control over the cooling rate, which is a common task in

process design. These process characteristics combined with the interesting wetting behavior open up possibilities for applications where large quantities are necessary and polydispersity is acceptable, as for example in tissue engineering or catalysis. Moreover, such particles could be used to study particle-cell interactions with specific surface textures, which is an ongoing area of research.[1d]

4. Experimental Section

Materials: All chemicals were used without further purification unless otherwise stated. Arachidic acid ($CH_3(CH_2)_{18}COOH$) was purchased from Alfa Aesar (98% purity). The surfactant CTAB ($CH_3(CH_2)_{15}N(CH_3)_3Br$) was purchased from Aldrich. Styrene was chosen as monomer because it has very low solubility in water and its polymerized form was soluble in the monomer liquid. The former was necessary for the suspension polymerization procedure and the latter was required to avoid phase segregation within a droplet.[5] Styrene was purchased from Merck (stabilized for synthesis). Free-radical initiator 2,2′-Azobis(2-methylpropionitrile) (AIBN, $(CH_3)_2C(CN)N{=}NC(CH_3)_2CN$) was purchased from Fluka (purity ≥ 98.0%). Ultrapure water with a resistance of at least 18.2 MΩ cm (Millipore Simplicity) was used to prepare aqueous solutions.

Particle Preparation: For prepolymerization of the styrene monomer phase, a mixture of arachidic acid (15 mg), AIBN (c_{AIBN} = 1 wt% = 10 mg) and styrene (1 g) was treated at 70 °C for 40 min in a silicone oil bath under vigorous stirring. An emulsion was then created by dropwise addition of hot prepolymerized monomer (0.7 g) to ultrapure water (50 mL) at 70 °C in a 100 mL three-neck, round-bottomed flask, and vigorous shaking. Suspension polymerization was carried out at 70 °C and 300 rpm for different periods of time between 110 and 150 min. Every 3 min, a sample of 1 mL solution was extracted from the hot emulsion and immediately added to a 3 mL glass vial containing a 20 °C cold aqueous solution of the cationic surfactant CTAB (1 mL, 2 mmol L^{-1}). The vessel was then placed in a 20 °C water bath to cool down and left quiescent for several days. When polymerization was completed, the particles were repeatedly washed in ethanol. For the investigation of the required polymerization times, the radical initiator concentration c_{AIBN} was varied from 1 to 3 wt% and the temperatures were altered from 60 to 80 °C according to Table 1 and polymerization times were adjusted. For contact angle measurements, an up-scaled version of the typical preparation procedure was conducted in order to produce more material. Instead of 1 mL the complete suspension was removed from the reaction vessel by means of a 50 mL syringe and a flexible tube and was then added to an aqueous CTAB solution (50 mL, 2 mmol L^{-1}) and kept at a temperature of 15 °C in a metal bowl. The flat-bottomed metal bowl (12.5 cm in diameter) was placed in the water bath of a thermostat at 15 °C to ensure fast cooling.

Influence of the Cooling Rate: A typical particle preparation was conducted by withdrawing 5 mL instead of 1 mL samples from the hot emulsion followed by immediate addition to a 25 mL glass vessel containing aqueous CTAB solution (5 mL, 2 mmol L^{-1}). Prior to the addition, the CTAB solution was cooled to 20, 15, or 0 °C and kept in a water or ice bath during and after the addition of the emulsion. Temperature inside the CTAB solution was recorded using a thermocouple.

Viscosity Measurements: Polymer solutions were prepared by bulk polymerization of styrene (7 g) containing AIBN (70 mg) and arachidic acid (105 mg) at 70 °C in a silicone oil bath under vigorous stirring. After 100, 113, 128, 143, or 160 min samples of 1 mL were extracted from the reaction mixture, rapidly cooled and stored in ice to prevent further polymerization. Rheological measurements were carried out on the same day on an Anton Paar Rheometer (MCR302) using a cone-plate geometry (plate diameter: 25 mm, cone angle: 1°) in rotation with a controlled shear rate of 100 s^{-1}. In a single measurement, the viscosity of a sample of 100 µL was measured while the temperature increased from 20 to 70 °C at a rate of 0.5 °C s^{-1}. Every measurement was performed twice.

Optical Microscopy: Particle suspensions were observed 3 days after synthesis using an Olympus IX70 inverted optical microscope.

Scanning Electron Microscopy and Focused Ion Beam Milling: For sample preparation, a droplet of particle suspension was placed on a silicon wafer and water was allowed to evaporate. Before observation, all samples were sputter-coated with a thin layer of gold. Scanning electron microscopy (SEM) and focused ion beam (FIB) milling were performed on a Zeiss Crossbeam 550. SEM images were recorded at an accelerating voltage of 5 kV with a working distance of 5 mm using a secondary electron detector. FIB-milling was performed with a gallium ion beam at 30 kV and 3 nA. FIB-images were recorded at 30 kV and 50 pA.

Contact Angle Hysteresis: Particle films were obtained by placing a drop of a suspension of the washed polystyrene particles in ethanol onto a salinized glass slide. The solvent was allowed to evaporate and the procedure was repeated until a continuous layer of particles had formed. Optical contact angle measurements with drop contour analysis were performed on a Dataphysics OCA35 instrument with an electrical dosing unit using ultrapure water of 18.2 MΩ cm resistance. Dynamic advancing and receding contact angles were measured following a procedure described in the literature.[18] A 3 µL droplet was placed on the sample surface keeping the needle tip inside the droplet. In a single step, 40 µL of water were dispensed and subsequently withdrawn from the droplet with a flow rate of 0.05 µL s^{-1}. Advancing and receding contact angles were analyzed between 3 and 10 µL because in that range the influences of gravitation and the distortion of the needle are negligible. Each sample surface was analyzed five times. The surface was allowed to dry in between measurements.

Acknowledgements

The authors thank Sebastian Thumbach (University of Augsburg) for performing light microscopy and Yvonne Gombert (ETH Zurich) for proofreading.

Open access funding enabled and organized by Projekt DEAL.

Conflict of Interest

The authors declare no conflict of interest.

Data Availability Statement

Research data are not shared.

Keywords

interfacial instability, microparticles, morphology, surface texture, surfactants

Received: April 16, 2021
Revised: June 8, 2021
Published online: July 20, 2021

[1] a) F. Caruso, *Adv. Mater.* **2001**, *13*, 11; b) S. Xu, Z. Nie, M. Seo, P. Lewis, E. Kumacheva, H. A. Stone, P. Garstecki, D. B. Weibel, I. Gitlin, G. M. Whitesides, *Angew. Chem., Int. Ed.* **2005**, *44*, 724; c) M. Björnmalm, J. Cui, N. Bertleff-Zieschang, D. Song, M. Faria, M. A. Rahim, F. Caruso, *Chem. Mater.* **2016**, *29*, 289; d) S. Mitragotri, J. Lahann, *Nat. Mater.* **2009**, *8*, 15.

[2] a) Y. Wang, L. Shang, G. Chen, C. Shao, Y. Liu, P. Lu, F. Rong, Y. Zhao, *Appl. Mater. Today* **2018**, *13*, 303; b) N. Doshi, S. Mitragotri, *PLoS One* **2010**, *5*, e10051; c) K. Saralidze, L. H. Koole, M. L. W. Knetsch, *Materials* **2010**, *3*, 3537; d) G. Sharma, D. T. Valenta, Y. Altman, S. Harvey, H. Xie, S. Mitragotri, J. W. Smith, *J. Controlled Release* **2010**, *147*, 408; e) M. Cooley, A. Sarode, M. Hoore, D. A. Fedosov, S. Mitragotri, A. Sen Gupta, *Nanoscale* **2018**, *10*, 15350; f) X. Zhu, C. Vo, M. Taylor, B. R. Smith, *Mater. Horiz.* **2019**, *6*, 1094; g) J. A. Champion, Y. K. Katare, S. Mitragotri, *J. Controlled Release* **2007**, *121*, 3.

[3] G. A. Silva, P. Ducheyne, R. L. Reis, *J. Tissue Eng. Regener. Med.* **2007**, *1*, 4.

[4] a) J.-H. Yang, Y.-S. Han, J.-H. Choy, *Thin Solid Films* **2006**, *495*, 266; b) F. Magalhães, R. M. Lago, *Sol. Energy* **2009**, *83*, 1521.

[5] M. T. Gokmen, F. E. Du Prez, *Prog. Polym. Sci.* **2012**, *37*, 365.

[6] a) R. Granek, R. Ball, M. Cates, *J. Phys. II* **1993**, *3*, 829; b) C. Solans, D. Morales, M. Homs, *Curr. Opin. Colloid Interface Sci.* **2016**, *22*, 88; c) J. Santana-Solano, C. M. Quezada, S. Ozuna-Chacón, J. L. Arauz-Lara, *Colloids Surf., A* **2012**, *399*, 78; d) J. C. López-Montilla, P. E. Herrera-Morales, S. Pandey, D. O. Shah, *J. Dispersion Sci. Technol.* **2002**, *23*, 219.

[7] a) J. Zhu, N. Ferrer, R. C. Hayward, *Soft Matter* **2009**, *5*, 2471; b) J. Zhu, R. C. Hayward, *J. Colloid Interface Sci.* **2012**, *365*, 275; c) Y. Wu, K. Wang, H. Tan, J. Xu, J. Zhu, *Langmuir* **2017**, *33*, 9889; d) K. H. Ku, J. M. Shin, H. Yun, G.-R. Yi, S. G. Jang, B. J. Kim, *Adv. Funct. Mater.* **2018**, *28*, 1802961.

[8] a) N. Denkov, S. Tcholakova, I. Lesov, D. Cholakova, S. K. Smoukov, *Nature* **2015**, *528*, 392; b) S. Guttman, Z. Sapir, M. Schultz, A. V. Butenko, B. M. Ocko, M. Deutsch, E. Sloutskin, *Proc. Natl. Acad. Sci. USA* **2016**, *113*, 493.

[9] a) I. Lesov, Z. Valkova, E. Vassileva, G. S. Georgiev, K. Ruseva, M. Simeonov, S. Tcholakova, N. D. Denkov, S. K. Smoukov, *Macromolecules* **2018**, *51*, 7456; b) O. Marin, M. Deutsch, D. Zitoun, E. Sloutskin, *J. Phys. Chem. C* **2019**, *123*, 28192.

[10] a) D. Volkmer, S. Tugulu, M. Fricke, T. Nielsen, *Angew. Chem., Int. Ed.* **2003**, *42*, 58; b) S. Tugulu, *Diploma Thesis*, Universität Ulm, Ulm **2002**; c) A. Roth, *Diploma Thesis*, Universität Bielefeld, Bielefeld **2003**.

[11] a) J. Zhu, R. C. Hayward, *Angew. Chem., Int. Ed. Engl.* **2008**, *47*, 2113; b) S. Liu, R. Deng, W. Li, J. Zhu, *Adv. Funct. Mater.* **2012**, *22*, 1692; c) N. Wang, Y. Liao, R. Deng, S. Liu, N. Cao, B. Tan, J. Zhu, X. Xie, *Soft Matter* **2012**, *8*, 2697; d) S. Liu, M. Cai, R. Deng, J. Wang, R. Liang, J. Zhu, *Korea Aust. Rheol. J.* **2014**, *26*, 63.

[12] V. B. Fainerman, D. Vollhardt, A. Roth, M. Fricke, D. Volkmer, *J. Phys. Chem. B* **2004**, *108*, 16163.

[13] B. Brooks, *Chem. Eng. Technol.* **2010**, *33*, 1737.

[14] S. Koltzenburg, M. Maskos, O. Nuyken, *Polymere: Synthese, Eigenschaften und Anwendungen*, Springer, Berlin Heidelberg **2013**.

[15] a) C. Bawn, R. Freeman, A. Kamaliddin, *Trans. Faraday Soc.* **1950**, *46*, 1107; b) W. M. Kulicke, R. Kniewske, *Rheol. Acta* **1984**, *23*, 75.

[16] B. Hager, G. Berry, *J. Polym. Sci., Polym. Phys. Ed.* **1982**, *20*, 911.

[17] a) C. W. Extrand, *Langmuir* **2002**, *18*, 7991; b) J. Wang, Y. Wu, Y. Cao, G. Li, Y. Liao, *Colloid Polym. Sci.* **2020**, *298*, 1107.

[18] T. Huhtamaki, X. Tian, J. T. Korhonen, R. H. A. Ras, *Nat. Protoc.* **2018**, *13*, 1521.